Identifying how future climate and land use/cover changes impact streamflow in Xinanjiang Basin, East China

Guo, Yuxue; Fang, Guohua; Xu, Yue Ping; Tian, Xin; Xie, Jingkai

DOI
10.1016/j.scitotenv.2019.136275

Publication date
2020

Document Version
Accepted author manuscript

Published in
Science of the Total Environment

Citation (APA)
Guo, Y., Fang, G., Xu, Y. P., Tian, X., & Xie, J. (2020). Identifying how future climate and land use/cover changes impact streamflow in Xinanjiang Basin, East China. *Science of the Total Environment*, *710*, Article 136275. https://doi.org/10.1016/j.scitotenv.2019.136275

Identifying how future climate and land use/cover changes impact streamflow in Xinanjiang Basin, East China

Yuxue Guo[1], Guohua Fang[2], Yue-Ping Xu[1*], Xin Tian[3], Jingkai Xie[1]

[1] Institute of Hydrology and Water Resources, Civil Engineering and Architecture, Zhejiang University, Hangzhou, 310058, China

[2] College of Water Conservancy and Hydropower Engineering, Hohai University, Nanjing, 210098, China

[3] Department of Water Management, Faculty of Civil Engineering and Geosciences, Delft University of Technology, Delft, 2623CN, Netherlands

[*]Corresponding author. E-mail address: yuepingxu@zju.edu.cn

Graphical Abstract

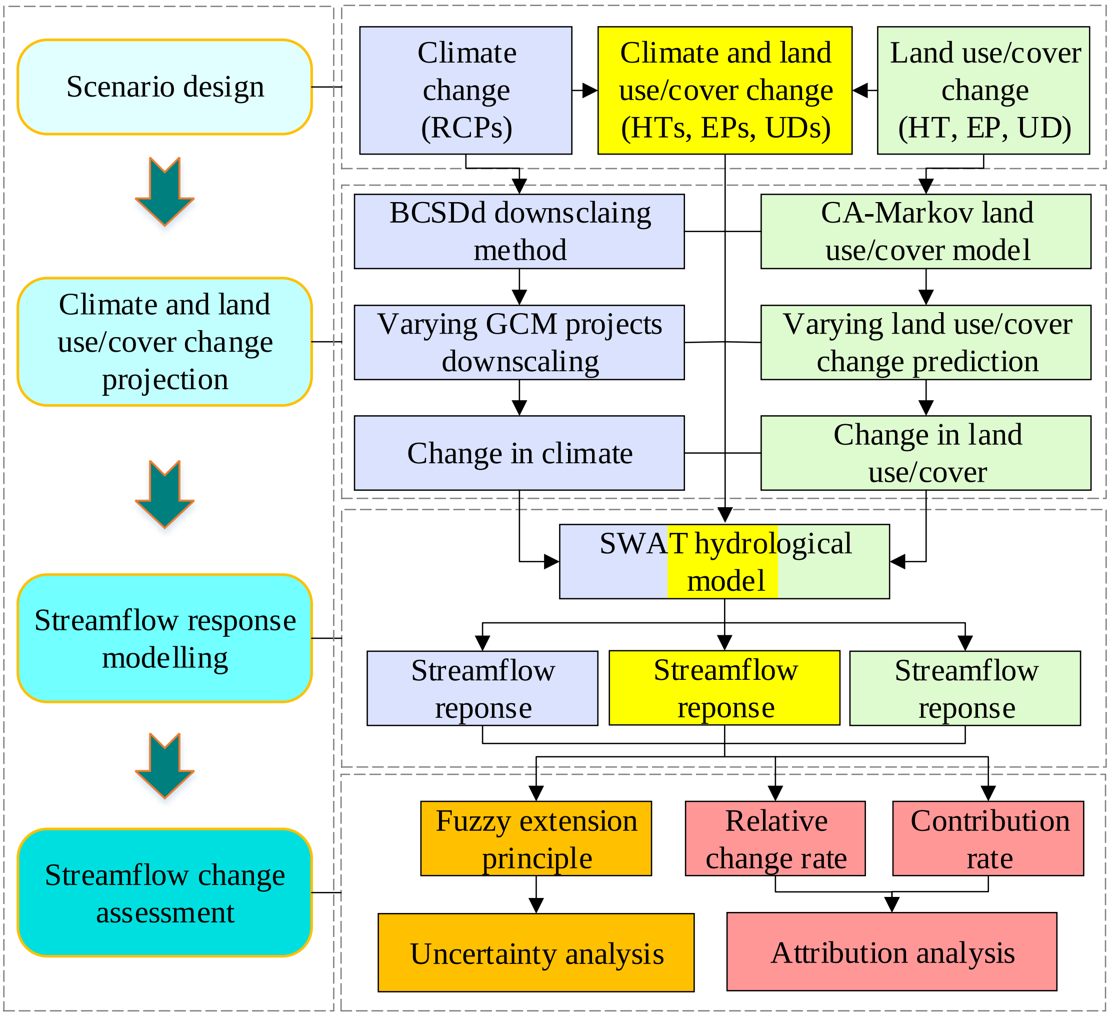

Abstract

Climate and land use/cover changes are the main factors altering hydrological regimes. To understand the impacts of climate and land use/cover changes on streamflow within a specific catchment, it is essential to accurately quantify their changes given many possibilities. We propose an integrated framework to assess how individual and combined climate and land use/cover changes impact the streamflow of Xinanjiang Basin, in East China, in the future. Five bias-corrected and downscaled General Circulation Model (GCM) projections are used to indicate the inter-model uncertainties under three Representative Concentration Pathways

(RCPs). Additionally, three land use/cover change scenarios representing a range of tradeoffs between ecological protection (EP) and urban development (UD) are projected by Cellular Automata - Markov (CA-Markov). The streamflow in 2021-2050 is then assessed using the calibrated Soil and Water Assessment Tool (SWAT) with 15 scenarios and 75 possibilities. Finally, the uncertainty and attribution of streamflow changes to climate and land use/cover changes at monthly and annual scale are analyzed. Results show that while both land use/cover change alone and combined changes project an increase in streamflow, there is a disagreement on the direction of streamflow change under climate change alone. Future streamflow may undergo a more blurred boundary between the flood and non-flood seasons, potentially easing the operation stress of Xinanjiang Reservoir for water supply or hydropower generation. We find that the impacts of climate and land use/cover changes on monthly mean streamflow are sensitive to the impermeable area (IA). The impacts of climate change are stronger than those induced by land use/cover change under EP (i.e., lower IA); and land use/cover change has a greater impact in case of UD (i.e., higher IA). However, changes in annual mean streamflow are mainly driven by land use/cover change, and climate change may decrease the influence attributed to land use/cover change.

Key words: multiple scenarios, climate change, land use/cover change, streamflow response, uncertainty, attribution.

1. Introduction

Efficient water resource management calls for a thorough understanding of changes in hydrological regime. Streamflow, as a primary component of the hydrological cycle, is widely believed to be affected mainly by climate and land use/cover changes (Alaoui et al., 2014; Ning et al., 2016; Abera et al., 2019). Climate change indirectly affects streamflow through changes in temperature, precipitation, and evaporation (Ruelland et al., 2012; Ahn and Merwade, 2014; Guo et al., 2019). Land use/cover change can significantly alter canopy interception, infiltration and evapotranspiration, which may eventually change the runoff volume, peak flow and flow routing time (Molina-Navarro et al., 2014; Zhang et al., 2017; Umair et al., 2019). Determining the individual or combined hydrological consequences of climate and land use/cover changes is a key for implementing effective measures for adaptation to climate change and for understanding the patterns of water use under different land use/cover policies (Wang et al., 2018; Clerici et al., 2019; Trolle et al., 2019).

Numerous studies have investigated the effects of climate change on streamflow (Gao et al., 2015; Chase et al., 2016). Particularly, since the publication of the Fifth Assessment Report of the Intergovernmental Panel on Climate Change (Cubasch et al., 2013), many studies have widely applied General Circulation Model (GCM) projections of the Coupled Model Intercomparison Project Phase 5 (CMIP5) to quantify how climate change impacts streamflow (Neupane et al., 2015; Eisner et al., 2017; Zheng et al., 2018). Results indicate that changes in streamflow show strong spatial variability under different Representative Concentration Pathways (RCPs). For example, Shrestha et al. (2018) found that RCP8.5 and RCP4.5 were responsible for a 19.5% and 24% decrease in future streamflow, respectively, in Thailand; but Wen et al. (2018) reported increases in streamflow along with the increasing temperature and precipitation under RCP2.6, RCP4.5, and RCP8.5 in the future, in southeast China. Another issue is the low resolution of GCM projections. Previous studies agree that the raw GCMs is too coarse to accurately describe the hydrological processes at regional scales (Chen and Frauenfeld, 2014; Sun et al., 2016; Guo et al., 2019), and thereby the conclusions on streamflow regime changes might not be reliable.

However, the extent to which streamflow responds to land use/cover change has not been fully investigated, and this response varies between catchments and between scenarios. Due to the acceleration of urbanization, the area of urban land has significantly increased, and consequently the area of impermeable surface has expanded, causing a sharp increase in streamflow at both long-term and short-term scales (Suriya and Mudgal, 2012; Li et al., 2018; Zhang et al., 2018). Ecological protection projects, e.g., the "Grain for Green" in China (Zhang et al., 2016), were initiated to increase the areas of forest and grassland, potentially resulting in an increase in vegetation coverage and a decline in surface streamflow (Zuo et al., 2016; Wang et al., 2019a; Yang et al., 2019). Some findings, however, have suggested that forest transforming to farmland and grassland could cause increases in mean annual streamflow (Shi, 2013). Accordingly, determining not only the impact of climate change on hydrology but also how different land use/cover management policies affect streamflow is vital for better managing water resources.

Recently, the joint effects of climate and land use/cover change on hydrology have been a main research focus (Liu et al., 2009; Kim et al., 2013; Zhang et al., 2017). Results show the complex and non-additive interactions between streamflow and climate and land use/cover change. Some studies found that streamflow alteration involved the superposition of the effects of climate and land use/cover changes, and land use/cover change was a dominant factor (Liu et al., 2009; Yin et al., 2017b), while some revealed that climate change was more dominant (Kim et al., 2013; Woldesenbet et al., 2018); Other studies also reported that climate change and land use/cover change each contributed 50% to streamflow variation (Wei et al., 2010). The abovementioned studies argue that the effects of climate and land use/cover changes on streamflow vary spatially. To understand the impacts of climate change and land use/cover management on streamflow, it is essential to accurately assess future changes within a specific catchment under diverse conditions. Nevertheless, few studies have attempted to combine varying land use/cover with varying climatic conditions for an uncertain future. Thus, an in-depth study on streamflow response to multiple climate and land use/cover change scenarios is needed.

The Xinanjiang is the main water source for riverside residents in Anhui and Zhejiang provinces. Studies investigating climate change in Xinanjiang Basin have noted that the annual streamflow showed an obvious increasing trend during a historical period due to the heavy rains and mountainous terrain (Zheng et al., 2015; Pan et al., 2018). In recent years, land use/cover in this basin has undergone dramatic changes because of urbanization and specific land use/cover policies; however, few studies have investigated how land use/cover change has affected streamflow. A better understanding of streamflow response driven by climate and land use/cover changes in Xinanjiang Basin would be beneficial for flood defense and hydropower utilization of Xinanjiang Reservoir. We aim to systematically investigate the individual and combined effects of climate and land use/cover changes on future streamflow in Xinanjiang Basin. Specifically, the Bias Correction and Spatial Disaggregation daily (BCSDd) downscaled CMIP5 GCM projections and land use maps simulated by the Cellular Automata - Markov (CA-Markov) model are employed to drive a Soil and Water Assessment Tool (SWAT) hydrological model and to project streamflow under diverse scenarios. Then, the streamflow uncertainty is evaluated at various levels using the fuzzy extension principle, while the individual and combined effects of climate and land use/cover changes on streamflow are analyzed with the relative change rate (RCA) and contribution rate.

2 Materials and methods

2.1 Study area

The Xinanjiang is the upstream part of the Qiantang River located in eastern China and has a total length of 323 km with an area of 11,503 km^2, as shown in Fig. 1. Three tributaries, the Hengshui River, the Shuaishi River, and the Lian River, flow into the main stream of Xinanjiang. The average annual temperature in Xinanjiang Basin is between 15.4 ℃ and 16.4 ℃, whereas the average annual precipitation is between 1280 mm and 1700 mm. The basin is dominated by a typical subtropical humid monsoon climate. The wet season (March to July) accounts for approximately 74% of the annual streamflow, while the dry season (from August to February) takes up the remaining 26%. Various landscapes, such as plains and mountains, are spatially distributed in the basin. Forest and grassland are the most widely distributed types, and cultivated land is concentrated at the periphery of urban land. Xinanjiang Reservoir is located downstream of Xinanjiang Basin, and is the first domestically designed and constructed reservoir in China, used mainly for hydropower generation for East China Region including Shanghai, Jiangsu, Anhui, and Zhejiang provinces, as presented in Fig. 1.

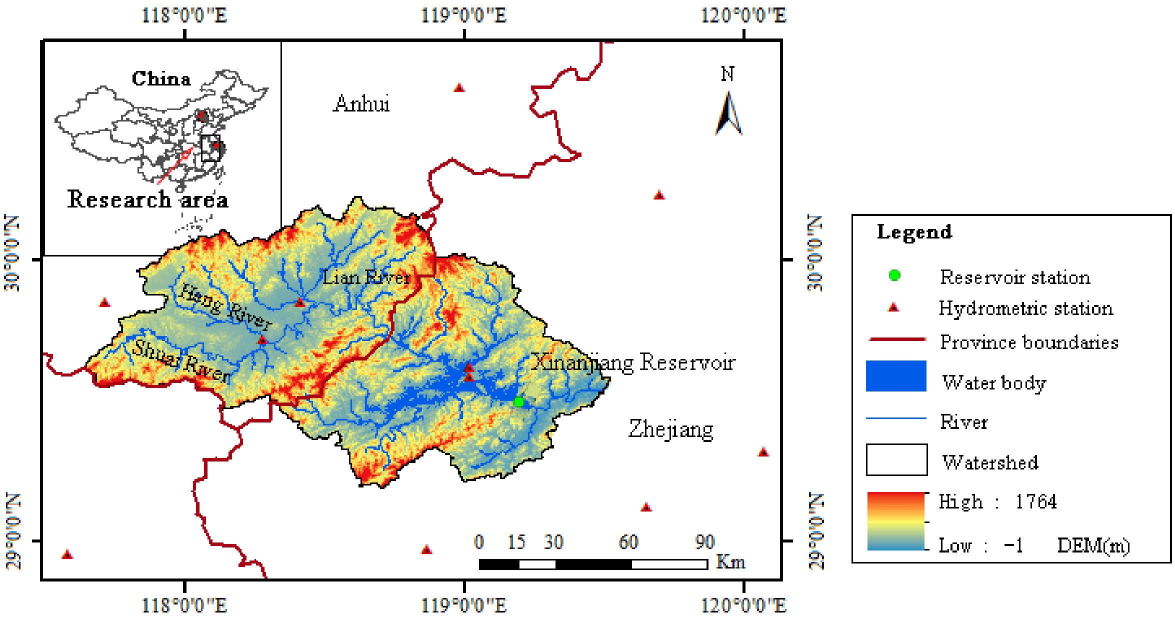

Fig. 1. Geographic location of Xinanjiang Basin.

2.2 Data collection

The observed meteorological data from 1976 to 2005 here are obtained from the National Meteorological Information Center of China (http://data.cma.cn) and these data comprise the daily precipitation, temperature, solar radiation, wind speed, and relative humidity, which are collected at nine hydrometric stations including Ningguo, Huangshan, Linan, Qimen, Tunxi, Chunan, Jinhua, Yiwu, and Quzhou, as shown in Fig. 1. The GCM climate projections are provided by the Earth System Grid Federation (https://esgf-node.llnl.gov), and these data include the daily precipitation and average, maximum and minimum temperature in 1976-2005 and 2021-2050. Five Coupled Model Inter-comparison Project Phase 5 (CMIP5) GCMs, namely Cnrm-cm5, Gedl-esm2m, Ipsl-cm5a-lr, Miroc-esm-chem, and Noresm1-m are used due to their good performance in climate simulation in China (Wen et al., 2018; Yang et al., 2019). More details on GCMs can be found in Supplementary information A1.

Geospatial data includes digital elevation model (DEM), land use/cover and soil map data. The DEM map at 90 m resolution used for defining streams and boundaries of sub-basins is provided by the Geospatial Data Cloud of China (http://www.gscloud.cn). The 30 arc-second soil map is originally derived from the Cold and Arid Regions Sciences Data Center at Lanzhou (http://westdc.westgis.ac.cn). Land use/cover maps at a 1km resolution for 1995, 2005 and 2015 from the Resource and Environment Data Cloud Platform of China (http://www.resdc.cn) are used to estimate the effect of land use/cover change over this period. The land use/cover here is reclassified into six classes for the SWAT model, namely forest, grassland, cultivated land, urban land, water body, and unused land.

The Zhejiang Design Institute of Water Conservancy & Hydro-electric Power provides the monthly inflow of Xinanjiang Reservoir from 1976 to 2005.

2.3 Methodology

We propose an integrated and systematic framework to assess how future climate and land use/cover changes impact streamflow using Xinanjiang Basin as a case study. This approach combines 1) scenario design involving individual and combined climate and land use/cover change; 2) climate and land use/cover change projection, where GCM projections are downscaled by the BCSDd method, and land use/cover maps are simulated by the CA-Markov model; 3) streamflow response modelling under uncertainty; 4) streamflow assessment including uncertainty, monthly and annual attribution analysis. In this study, the baseline is in the period of 1976-2005 and the future is in the period of 2021-2050. We assume that there were no significant changes in land use/cover before 2005, and therefore use the land use/cover in 1995 as the representative land use/cover in the baseline period. Regarding to the land use/cove change scenarios, we use the land use/cover in 2025 as the representative land use/cover in the future period.

2.3.1 Scenario design

We select three RCP scenarios to assess how different emission scenarios impact streamflow, namely RCP2.6, RCP4.5 and RCP8.5. These three scenarios represent the low, medium and high emission of greenhouse gases, respectively, which are named according to their total radiative forcing in 2100 relative to pre-industrial values (+2.6, +4.5 and +8.5 W/m^2, respectively).

Three land use/cover scenarios that represent a range of tradeoffs between ecological protection and urban development are proposed to identify how different land use/cover policies affect streamflow, namely Historical Trend (HT), Ecological Protection (EP) and Urban Development (UD) scenarios. The three scenarios all assume that future land use/cover demands are based on the historical trend, but vary with specific characteristics of each scenario.

(1) HT Scenario. This scenario emphasizes there would be no interventional policy made for land use/cover changes in the future.

(2) EP Scenario. This scenario also aims to maintain a greater vegetation coverage rate and develop the ecological land (forest and grassland) area, which forbids the transformation of the ecological land to other land use/cover types. It is generally used to represent future land use/cover with a low impermeable area (IA).

(3) UD Scenario. In contrast with the EP scenario, this scenario not only requires the urban land not to be transformed to other land use/cover types, but also encourages the other types to be converted to urban land. To some extent, this scenario reflects the current maximum economic profit and ignores ecological protection. It is generally used to represent future land use/cover with a high IA.

In terms of the combined climate and land use/cover change scenarios, we assemble RCPs with HT as HTs (i.e., HT2.6, HT4.5, and HT8.5); EP as EPs (i.e., EP2.6, EP4.5, and EP8.5); UD as UDs (i.e., UD2.6, UD4.5, and UD8.5). Thus, different scenarios, 15 in total, are designed based on different climate and land use/cover changes. Accordingly, there are in total 75 possibilities by coupling 15 scenarios and 6 GCMs projections (5 GCM models and 1 multi-model ensemble means).

2.3.2 Bias correction of future climate data

To address the low-resolution problem of raw GCM projections at regional scales, the BCSDd method (Thrasher et al., 2012) is applied to establish empirical relationships between GCM-resolution climate variables and local climate and to reproduce the regional climate features. Generally, the BCSDd method includes two steps: 1) Bias correction. Both daily raw GCM projections and observations are first re-gridded to a certain coarse resolution by the inverse distance weighted (IDW) method (Mito et al., 2011). The bias-corrected value for a raw daily GCM projection is obtained by using the Cumulative Distribution Function (CDF) for the GCM and observation to determine the same quantile associated with the projection. Particularly, bias correction covers a common time period for observations and GCM. 2) Spatial downscaling. The daily bias-corrected values are spatially disaggregated to a high-resolution grid by the sonographic mapping system (SYMAP) interpolating (Shepard, 1984). The high-resolution value is then used to calculate the correction factors between the observations and high-resolution GCM projections, specifically, multiplication for precipitation and plus for temperature. Further, the index of root mean squared error (RMSE), mean of bias (MBIAS), standard deviation of bias (SBIAS), and correlation coefficient (R) are used to examine the accuracy of the downscaled results of the BCSDd method. Note that the low the MBIAS, SBIAS, and RMSE values are, the better the results, whereas a larger R are preferable. The details on statistic variable equations can be found in Supplementary Materials A2.

2.3.3 CA-Markov land use/cover modelling

Land use/cover models are commonly divided into three categories, namely quantitative, space and combination models. The CA-Markov model (Zhao et al., 2019) linking CA (a space model) and Markov Chain (a quantitative model) is adopted to project the land use/cover change in this study. The Markov model (Sang et al., 2011) describes the likelihood of change from one state to another based on a transition probability matrix achieved with the following equation in the Markov Chain process:

$$S_{t+1} = P \times S_t \tag{1}$$

where S_t and S_{t+1} are the land use/cover status at time of t and $t+1$, respectively; P is the transition probability matrix in a state that is calculated as follows:

$$P = \begin{vmatrix} P_{11} & P_{12} & \cdots & P_{1n} \\ P_{21} & P_{22} & \cdots & P_{2n} \\ \cdots & \cdots & \cdots & \cdots \\ P_{n1} & P_{n2} & \cdots & P_{nn} \end{vmatrix} \tag{2}$$

where $\sum_{i=1}^{n} P_{ij} = 1$, $0 \le P_{ij} \le 1$, P_{ij} is the transition probability from land use/cover type i to type j; and *n* is the number of land use/cover types in the target area.

Due to lack of spatial parameters, the Markov Chain model is unable to identify the spatial variability in land use/cover (Firozjaei et al., 2019). By adding an element of spatial contiguity as well as information on the likely spatial distribution of transitions to Markov chain analysis, the CA model makes it possible to simulate spatial and temporal evolution of land use/cover using the CA-Markov model. The CA model can be defined as follows:

$$S_{t+1} = f\left(S_t, N\right) \tag{3}$$

where N is the cellular field; and f is the transition rule of the cellular states.

There are two cores in the CA-Markov model, the transition probability matrix from baseline to potential land use/cover change for Markov and the suitability map built according to the driving force analysis of land use/cover change for CA, and their combination contributes to a better land use/cover simulation. To distinguish the differences on land use/cover between scenarios, constraint maps under different scenarios were expressed using the Boolean map, with suitable transformation areas coded with one and others coded with zero (Behera et al., 2012). Then, the sub-suitability maps coupled with the constraint maps are prepared as the final suitability map for different scenarios. In this study, we use the land use/cover in 2025 as the representative land use/cover in the future period. Details on the specific processes of CA-Markov modelling land use/cover in 2025 under different scenarios can be found in Supplementary materials A3. Before prediction, the Kappa index (Mitsova et al., 2011) is adopted to gauge the degree of agreement between the simulated and observed land use/cover map. The land use/cover simulation is acceptable if Kappa>0.4.

2.3.4 SWAT hydrological model

Hydrological modelling methods are widely used to quantify the effects of climate and land use/cover change (Woldesenbet et al., 2018). The Variable Infiltration Capacity (Liang et al., 1994), SWAT (Arnold et al., 1998), Hydrologic Simulation Program-Fortran (Deliman et al., 1999) and Water Erosion Prediction Project (Flanagan et al., 2001) are the commonly used hydrological models, among which the SWAT model has been successfully used in studies associated with climate change and land use/cover change. It is evident that the SWAT model has yielded high accuracy for short/long-term simulations of yearly and monthly mean streamflow (Zuo et al., 2016; Anand et al., 2018; Bhatta et al., 2019). Thus, we use the SWAT model to project future streamflow under diverse scenarios. In the SWAT model, a catchment will be divided into several sub-basins and then partitioned into hydrological response units (HRUs) according to the same land use/cover and soil type. The water flow in each HRU is simulated based on the water budget formula. See more details in Arnold et al. (1998).

In this study, ArcSWAT2012 running on an ArcGIS 10.2 platform is used for watershed delineation and sub-basin discretization. The Xinanjiang Basin is divided into 121 sub-basins and multiple HRUs according to the land use/cover, soil types, and slope classes. The slope of Xinanjiang Basin with a range from 0 to 10% is accounted for more than 90% of the whole basin. The procedures of parameter calibration, verification, and sensitivity analysis in the SWAT model can be conducted by the SWAT Calibration and Uncertainty Programs (SWAT-CUP) (Abbaspour et al., 2007). The sensitivity analysis of the parameters is determined by the t-statistics and the p-value. A larger absolute value of t-statistics and a smaller value of the p-value correspond to a more sensitive parameter. The coefficients of determination (R^2) (Woldesenbet et al., 2017) and Nash-Sutcliffe efficiency (NSE) (Dile et al., 2016) are used to quantify the goodness of model performance. The performance of hydrological simulation is considered to be acceptable if R^2>0.5 or NSE>0.5.

Discharge data during the period of 1976-2005 at one hydrological station (presented in Fig.1) located at upper dam site of Xinanjiang Reservoir is used for model sensitivity analysis, calibration and validation. First, under the land use/cover of 1995 and driven by the observed meteorological data during 1975-2005, the SWAT model is calibrated and validated on a monthly scale in 1976-1995 and 1996-2005. Further, the individual and combined effects of climate change and land use/cover change on streamflow are evaluated using the SWAT model.

2.3.5 Methods for streamflow change analysis

a) Fuzzy extension principle

As multiple drivers involve many uncertainties, identifying the uncertainty and range of predicted streamflow is beneficial for water management. Fuzzy set theory is able to handle uncertainty problems, especially one of which is associated with a lack of information at hand.

In this study, we use the fuzzy extension principle (Wambura et al., 2015) to evaluate the uncertainty in streamflow. The method uses a horizontal line, namely fuzzy alpha-level cut (α-cut), to describe the elements belonging to a particular certainty level from the membership function. The membership level may take any value ranging from zero to one:

$$\mu_A(x) = \begin{cases} 0 & if \;\; x \le a \\ \dfrac{x-a}{b-a} & if \;\; a < x \le b \\ \dfrac{c-x}{c-b} & if \;\; b < x \le c \\ 0 & if \;\; x \ge c \end{cases} \tag{4}$$

where $\mu_A(x)$ is the degree of membership of *x* in fuzzy subset *A*, $\mu_A(x)$=0 means no membership and $\mu_A(x)$=1 represents full membership; a and c stand for the lower and upper bounds, respectively, and b is the core of the fuzzy number.

The α-cut is the certainty level, which ranges between zero and one (Gonzalez et al., 1999). In general, a high α-cut corresponds to a higher confidence degree and a lower uncertainty level. Assume that the α-cut is assigned as 0%, 50% and 100%, the corresponding uncertainty levels will be 100%, 50% and 0%, respectively.

b) Relative change rate

The RCA (Wen et al., 2018) is defined as the ratio of changes in the outcome variable before and after considering the influence factors to the standard deviation of the outcome variable, which can directly compare the relative contribution on outcome variable between different influence factors. Thus, the RCA is a powerful tool to provide a better understanding of how different influence factors alter streamflow at monthly scale, and it can be calculated by the following formula:

$$\alpha_i = \left| \frac{d_i}{D_i} \right| \tag{5}$$

$$D_i = \sqrt{\frac{1}{N}\sum_{j=1}^{N}\left(Q_{ij} - \overline{Q_i}\right)^2} \tag{6}$$

$$d_i = \overline{Q_i} - \overline{q_i} \tag{7}$$

where α_i is the RCA of the mean monthly streamflow of the i^{th} month, D_i is the standard deviation of the mean monthly streamflow of the i^{th} month, d_i is the difference in mean annual streamflow of the i^{th} month between the basic and future periods, Q_{ij} is the mean monthly streamflow in different years in the baseline, $\overline{Q_i}$ and $\overline{q_i}$ are the mean annual streamflow of the i^{th} month in the baseline and future period, respectively; N is the number of years.

c) Contribution rate

When one driving factor varies and another remains constant, the simulation results show the effects of the variable factor on the hydrological components (Yin et al., 2017a). The contribution rate can be used to directly separate the effects of climate and land use/cover changes on streamflow (Qiang et al., 2016). We use RCP2.6 and HT as an example here. The difference in streamflow between RCP2.6 ($Q_{RCP2.6}$) and the baseline (Q_b) can be regarded as the effect of RCP2.6 on streamflow change. Similarly, the difference in streamflow between HT2.6 ($Q_{HT2.6}$) and HT (Q_{HT}) can be regarded as the effect of RCP2.6 on streamflow change. Therefore, the impacts of RCP2.6 ($\Delta Q_{RCP2.6}$) on streamflow should be calculated by the following formula:

$$\Delta Q_{RCP2.6} = \frac{\left(Q_{RCP2.6} - Q_b\right) + \left(Q_{HT2.6} - Q_{HT}\right)}{2} \tag{8}$$

Furthermore, the effects of HT (ΔQ_{HT}) on streamflow can be determined by applying the difference between HT (Q_{HT}) and the baseline (Q_o) or between HT2.6 ($Q_{HT2.6}$) and HT ($Q_{RCP2.6}$):

$$\Delta Q_{HT} = \frac{\left(Q_{HT} - Q_b\right) + \left(Q_{HT2.6} - Q_{RCP2.6}\right)}{2} \tag{9}$$

The difference between streamflow in HT2.6 and the baseline represents the combined effects of RCP2.6 and HT on streamflow change. We find the combined effects ($\Delta Q_{HT2.6}$) are equal to the sum of the individual effects.

$$\Delta Q_{HT2.6} = Q_{HT2.6} - Q_b = \Delta Q_{RCP2.6} + \Delta Q_{HT} \tag{10}$$

Hence, the percentage contributions of RCP2.6 ($\eta_{RCP2.6}$) and HT (η_{HT}) to the variations in streamflow can be calculated as follows:

$$\eta_{RCP2.6} = \frac{\Delta Q_{RCP2.6}}{\Delta Q_{RCP2.6} + \Delta Q_{HT}} \times 100\% \tag{11}$$

$$\eta_{HT} = \frac{\Delta Q_{HT}}{\Delta Q_{RCP2.6} + \Delta Q_{HT}} \times 100\% \tag{12}$$

The quantitative contribution of the other climate and land use/cover change scenarios can also be determined by the above principle.

3. Results

3.1 Climate change under varying scenarios

We used the BCSDd method to correct and downscale the GCM temperature and precipitation during the period of 1976-2005 and 2021-2050 in Xinanjiang Basin. Table 1 shows the evaluation indexes between the raw and BCSDd downscaling of GCM projections from 1976 to 2005. It is clear that BCSDd downscaling can significantly correct the GCM temperature and precipitation. Specifically, all the performance indexes for precipitation are improved. For temperature, the values of RMSE and SBIAS are reduced by 0.42-1.10 °C and 0.32-0.71 °C, respectively, while the value of R is increased by 0.01-0.02; due to the bias correction of daily historical probability distribution function, the value of MBIAS is expected to be 0.

Table 1 Comparison of the evaluation indexes between the raw and BCSDd downscaling of GCMs from 1976 to 2005.

GCM		Precipitation (mm)				Temperature (°C)			
		RMSE	R	MBIAS	SBIAS	RMSE	R	MBIAS	SBIAS
Noresm1-m	Raw	10.16	0.10	0.39	10.16	2.37	0.97	-0.89	2.20
	BCSDd	5.86	0.80	-0.11	5.86	1.58	0.98	0.00	1.58
Miroc-esm-chem	Raw	9.76	0.07	1.16	9.69	2.61	0.97	1.60	2.06
	BCSDd	5.90	0.79	-0.12	5.90	1.75	0.98	0.00	1.76
Ipsl-cm5a-lr	Raw	9.84	0.09	0.89	9.80	2.08	0.97	-0.60	1.99
	BCSDd	6.23	0.78	-0.11	6.23	1.66	0.98	0.00	1.66
Gedl-esm2m	Raw	9.81	0.11	1.07	9.75	2.72	0.96	-1.36	2.36
	BCSDd	7.17	0.72	-0.13	7.17	1.65	0.98	0.00	1.65
Cnrm-cm5	Raw	10.60	0.10	-0.80	10.57	2.64	0.97	-1.85	1.88
	BCSDd	6.05	0.79	-0.15	6.05	1.54	0.98	0.00	1.54
Multi-model	Raw	8.65	0.17	0.54	8.63	1.71	0.98	-0.62	1.59
ensemble means	BCSDd	4.98	0.84	-0.12	4.98	1.27	0.99	0.00	1.27

Fig. 2 shows the temperature and precipitation over Xinanjiang Basin in 1971-2005 and 2021-2050. The mean annual temperature in the baseline period is 16.32 °C, while that in the future varies under different GCM projections. The mean annual temperatures of the Noresm1-m, Ipsl-cm5a-lr and Miroc-esm-chem models are significantly increased by 0.07-3.86 °C under RCPs, the Gedl-esm2m model are slightly decreased by 0.09-0.40 °C relative to the baseline period. The Cnrm-cm5 model has the exception that the mean annual temperature decreases under RCP2.6, but increases under RCP4.5 and RCP8.5. Not surprisingly, the mean annual temperature is expected to increase with increasing radiation intensity for all GCM projections, and the multi-model ensemble means under RCPs (solid markers) may experience an increase in mean annual temperature ranging from 0.76°C to 1.20 °C. Additionally, Xinanjiang Basin has four distinct seasons both in the baseline and future periods. The differences in monthly temperature among RCPs are not significant.

The mean annual precipitation in 1976-2005 is 1598.61 mm, and will probably increase by 2.40-3.24% in 2021-2050. The multi-model ensemble range in monthly precipitation is narrow and similar. However, the error bar indicating the multi-model ensemble range in monthly temperature shows the larger uncertainty under RCPs. Although GCMs do not all project an increased mean annual precipitation with increasing radiation intensity, the multi-model ensemble means anticipates positive increases in the mean annual precipitation by 44.07-45.08 mm under RCPs. There is a non-uniform distribution of mean monthly precipitation in Xinanjiang Basin. The precipitation in spring and summer accounts for 72.93% of the total precipitation in 1976-2005, and 72.03-72.72% in 2021-2050.

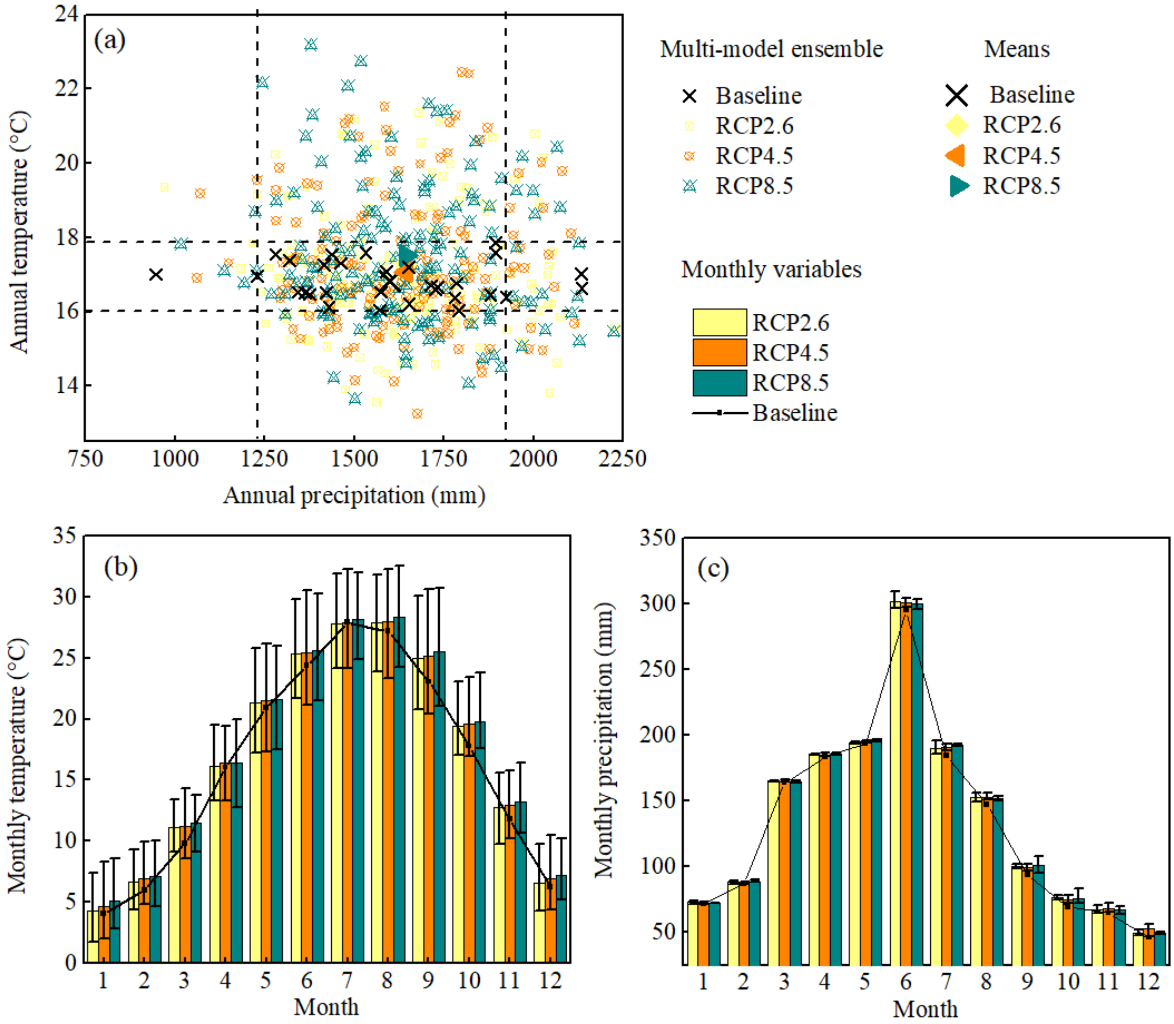

Fig. 2 Mean (a) annual temperature and precipitation, monthly (b) temperature and (c) precipitation averaged over Xinanjiang Basin projected by downscaled CMIP5 GCMs under different RCPs in 2021-2050. The error bars indicate the multi-model ensemble range.

3.2 Land use/cover change under varying scenarios

Here, the land use/cover map of 2015 was first predicted using the maps of 1995 and 2005. The simulated map of 2015 was compared to the observed map of 2015 to evaluate the reliability of the CA-Markov model, which was acceptable with a Kappa value of 0.68 for Xinanjiang Basin. Then, the CA-Markov model was applied to simulate the land use/cover changes under the three scenarios in 2025, as shown in Fig. 3.

By comparing the land use/cover simulation results of Xinanjiang Basin in 2025 relative to those in 1995, we can see that the spatial distributions of land use/cover under the three scenarios differ significantly. Under HT, the areas of forest, cultivated land and water body decrease from 1995 to 2025, while the areas of the other land use/cover types are all increased to varying degrees ranging from 43.84% to 516.28%. Under EP, forest and grassland are still the two dominant land use/cover types, contributing to a total increase of 5.48%. The area of water body declines slightly, and cultivated land has a large reduction of 51.70%. The urban area increases largely owing to the changeover of forest and cultivated land. Under UD, a sharp increase in urban land is observed with a value of 192.68%. The urban area increases largely due to the conversion of forest, grassland, and cultivated land. Overall, the areas of forest and grassland under EP are predicted to undergo the largest proliferation among all scenarios, while the area of urban land is the lowest. In contrast, the area of urban land under UD is obviously larger than those under the other two scenarios, while the areas of forest and grassland are the lowest. Land use/cover under HT has undergone changes because of urbanization following the historical trend, but less urbanization occurs than that under UD.

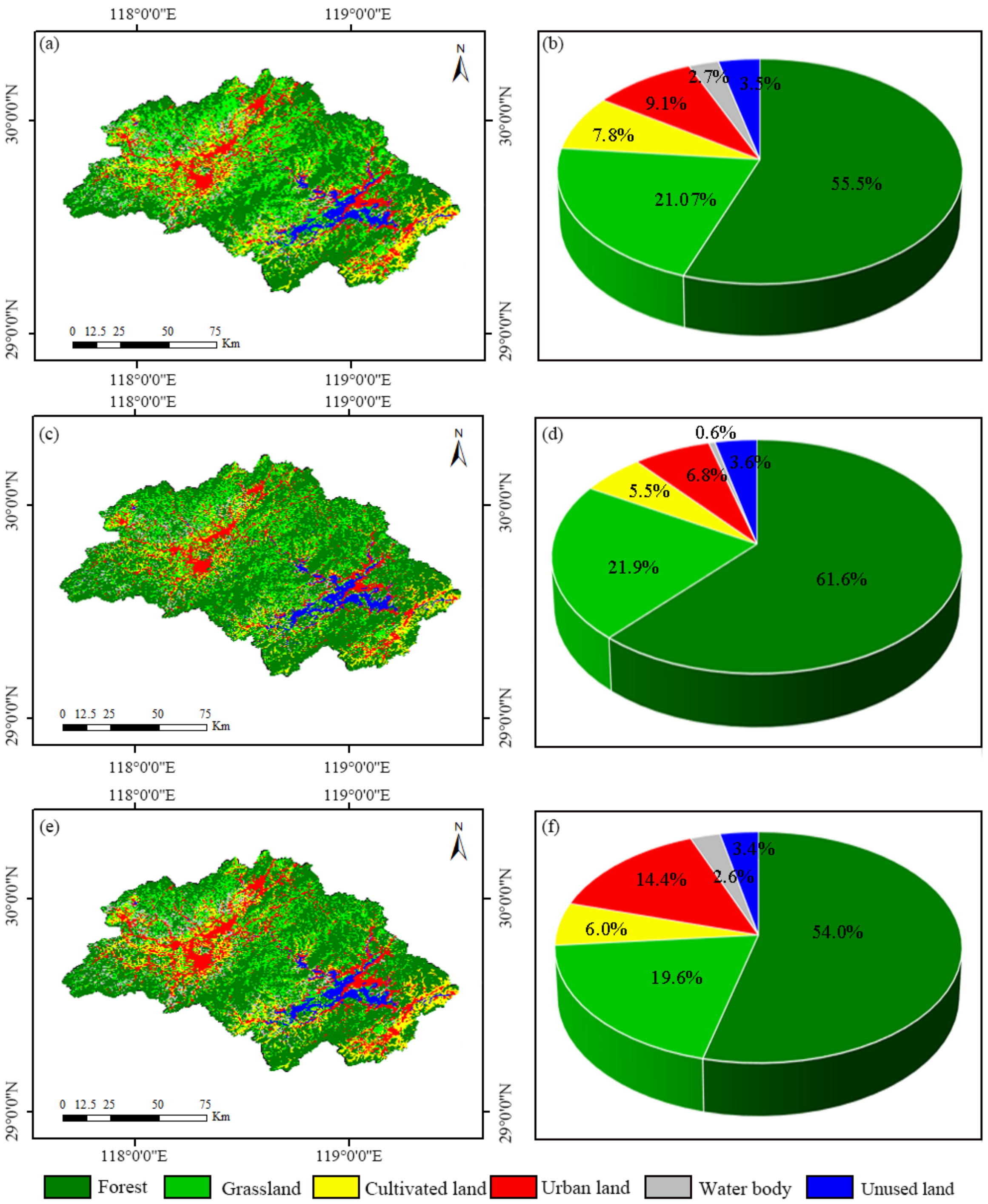

Fig. 3. Projected land use/cover maps in 2025 under (a) HT, (c) EP, and (e) UD scenarios, and proportions of area of each land use type under (b) HT, (d) EP, and (f) UD scenarios.

3.3 Sensitivity analysis, calibration and validation results of SWAT model

The results of global sensitivity analysis using SWAT-CUP are listed in Table 2, based on their ranking. ESCO, GW_DELAY, SURLAG, CH_S2, CH_K2, GWQMN, CN2, SLSUBBSN, SOL_Z, CANMX, SOL_AWC, and OV_N are the first 12 high sensitivity parameters for the simulated streamflow. Soil evaporation compensation factor ‘ESCO’ ranked the first, much higher than others. Table 2 shows that parameters representing groundwater return flow, soil properties, ground water, and surface runoff are sensitive. Therefore, accurate estimation of these parameters is important for streamflow.

Table 2 Parameter sensitivity analysis and calibration results for the SWAT model.

Parameter	Description	Sensitivity analysis		Calibration		
		t- statistics	*p*-value	Min	Max	Optimal
v_ESCO	Soil evaporation compensation factor	-4.22	0	-1.00	1.00	0.40
r_GW_DELAY	Groundwater delay time (days)	-3.01	0	-120.00	100.00	-54.00
v_SURLAG	Surface water lag	-2.7	0.01	0.05	30.00	3.05
v_CH_S2	Average slope of the main channel in the sub-basin (m/m)	2.23	0.03	-0.20	0.10	0.07
v_CH_K2	Effective hydraulic conductivity in main channel alluvium (mm/h)	2.04	0.04	-0.20	0.10	0.01
r_GWQMN	Threshold depth of water in the shallow aquifer required for return flow (mm)	-2.02	0.04	0.00	2.00	1.40
v_CN2	SCS runoff curve number for moisture condition II	-1.62	0.11	-0.20	0.20	-0.16
r_SLSUBBSN	Average slope length	-1.4	0.16	0.00	100.00	50.00
v_SOL_Z	Soil depth (mm)	1.34	0.18	-	-	-
v_CANMX	Maximum storage capacity(mm)	1.33	0.19	0.00	0.10	0.07
v_SOL_AWC	Base flow alpha factor (mm/mm)	1.01	0.31	-	-	-
v_OV_N	Manning's "n" value for overland flow	0.91	0.36	0.01	1.00	0.11

The SWAT model was calibrated and validated on a monthly scale in 1976-1995 and 1996-2005, respectively. Results show that the observed and SWAT simulated discharge fit well with values of R^2=0.92 and NSE=0.93 for the calibration period, and R^2=0.90 and NSE=0.92 for the validation period. The hydrological model captures the low flows and some peaks very well, in particular the highest peak. The simulated and observed inflow of Xinanjiang Reservoir over the period 1976-2005 for calibration and validation can be found in Supplementary materials A4. The derived parameter values obtained from calibration and confirmation analyses were incorporated with the SWAT database for further simulations.

3.4 Streamflow response modeling under multiple scenarios

We then projected the long-term (2021-2050) streamflow under climate change alone, land use/cover change alone, and their combination using the calibrated SWAT model and 75 possibilities. Two widely used methods in mainstream literatures, Mann-Kendall-*Sen* (MK-*Sen*) trend test (Mann, 1945; Kendall, 1975) and Pettitt test (Pettitt, 1979) were adopted to analyze the trends and abrupt changes of the streamflow time series in this study, respectively. The test principle and results are provided in Supplementary materials A5-A6. These results show that almost every annual streamflow series show an increasing trend during 2021-2050, and only some possibilities have a significant increasing trend at 5% significance level. It can be found that streamflow abruptly changed around 2030s in Xinanjiang Basin in the future. The predicted streamflow at annual and monthly scales are shown in Fig. 4.

3.4.1 Under varying climate change scenarios

In 1976-2005, the mean annual streamflow is 334.86 m^3/s with a frequent fluctuation between dry and flood years. The mean annual streamflow in 2021-2050 is 334.32-356.35 m^3/s, with a variation of -0.16-6.42% relative to that in 1976-2005. All GCMs show an increasing trend in future streamflow under RCPs except the Miroc-esm-chem model under RCP2.6. This result occurs because the Miroc-esm-chem model sees the most pronounced warming with minimal rainfall under RCP2.6; thus, evapotranspiration increases, resulting in a decrease in streamflow. The annual streamflow has a slight fluctuation between dry and flood years, and especially for the multi-model ensemble means. This result indicates that the mean GCM projections will underestimate the probability of extreme flood and drought events.

Fig. 4 (b) shows an uneven distribution of mean monthly streamflow is expected in Xinanjiang Basin in both 1976-2005 and 2021-2050. In the flood periods from March to August, the mean streamflow is 541.77 m^3/s and the total streamflow accounts for 80.89% of the total streamflow in a year in 1976-2005. In 2021-2050, the difference in streamflow between dry and wet years might decline. In the flood periods, the mean streamflow is decreased by 0.73-6.70% compared to that in 1976-2005, while the total streamflow in this period accounts for 74.06-76.56% of the total streamflow, with a decline of 5.35-8.45%. Meanwhile, an increase in the monthly streamflow is observed in the dry periods and the mean streamflow is 159.18-184.87 m^3/s with an increase of 24.40-44.48% relative to that in 1976-2005; while the total streamflow in this period accounting for the total streamflow in a year is also increased by 22.67-35.77%. Overall, it is evident that a more blurred boundary between dry and wet periods may occur in the future. All GCMs project similar streamflow under RCPs at the monthly scale, which indicates that the streamflow in Xinanjiang Basin is affected mainly by precipitation rather than by temperature.

3.4.2 Under varying land use/cover change scenarios

Fig. 4 (c) and (d) show the annual and monthly streamflow variations under land use/cover change. The streamflow shows a similar increasing trend over the period of 2021-2050 under three land use/cover change scenarios, with a mean annual streamflow of 347.89-354.32 m^3/s. The areas of urban land use/cover significantly expand under UD, resulting in a sharp increase in IA, and the mean annual streamflow in 2021-2050 increases by 5.81% relative to that in 1976-2005. Because land use/cover has undergone dramatic changes due to urbanization during 2005-2015, the urban land increases under HT but its increase is still lower than that under UD. Therefore, the mean annual streamflow under HT is lower than that under UD with a variation of 4.00%. In EP, the vegetation coverage is the highest, but the mean annual streamflow is the lowest with a variation of 3.89%.

The maximum monthly streamflow is expected to decline by 55.78-90.32 m^3/s in June, which is similar to the pattern under climate change. The UD scenario has the largest monthly streamflow in June, indicating that a flood crisis might be induced by urban development. Additionally, an increase in the monthly streamflow is expected in the dry periods, and the minimum monthly streamflow in December is predicted to increase by 248.32-249.19 m^3/s. Overall, it is evident that a more blurred boundary can be observed between the flood and non-flood seasons under land use/cover change. The different distribution characteristics of monthly streamflow under land use/cover change can be divided into two periods. The monthly streamflow from January to June under UD is higher than that under the other two scenarios; in contrast, the monthly streamflow from August to December under UD is smaller than that under both HT and EP. Therefore, land use/cover change can affect not only the amount of annual average, but also the timing of streamflow in Xinanjiang Basin.

3.4.3 Under varying combined climate and land use/cover change scenarios

Fig. 4 (e) and (f) present the annual and monthly streamflow variations under combined climate and land use/cover changes. The streamflow shows an increasing trend over the period 2021-2050 under combined scenarios, with a mean annual streamflow of 335.92-364.07 m^3/s, and has an annual variation of 0.32-8.72% compared with that in 1976-2005. The mean annual streamflow under UDs is the largest, followed by that under HTs and EPs. Moreover, the alteration characteristics of annual streamflow are similar under different land use/cover changes. Regarding the same land use/cover change, the annual mean streamflow is not sensitive to increasing radiation intensity, and the annual fluctuation varies between the dry and flood year. The annual streamflow under the combined climate and land use/cover change is consistent with that under climate change alone, although the mean value is lower than that of individual land use/cover influence, and higher than that of individual climate change influence.

In the flood seasons from April to July, the streamflow accounts for the total streamflow decrease by 2.97-9.55% relative to that in 1976-2005. However, there is a disagreement on the direction of streamflow change in this period. The mean streamflow is 593.30-627.65 m^3/s with a decline of 1.42-6.82% under HTs and EPs, but the mean streamflow is changed by -2.52-3.40%

under UDs. A significant increase of 25.91-65.94% occurs in the non-flood seasons from October to January. This result also demonstrates that in the future under combined climate and land use/cover changes, a more blurred boundary between the flood and non-flood seasons may be expected. Then, we compared the streamflow between the combined scenarios and climate change alone and land use/cover change alone. A similar distribution pattern of monthly streamflow with that under individual land use/cover change can be observed. The monthly streamflow under UDs from January to June is higher than that under both EPs and HTs, while the monthly streamflow under UDs from August to October is lower. Under the same land use/cover change conditions, no significant difference can be detected among RCPs, which is similar to that under climate change alone. These results indicate that complex and non-additive interactions exist between streamflow and climate change and land use/cover change.

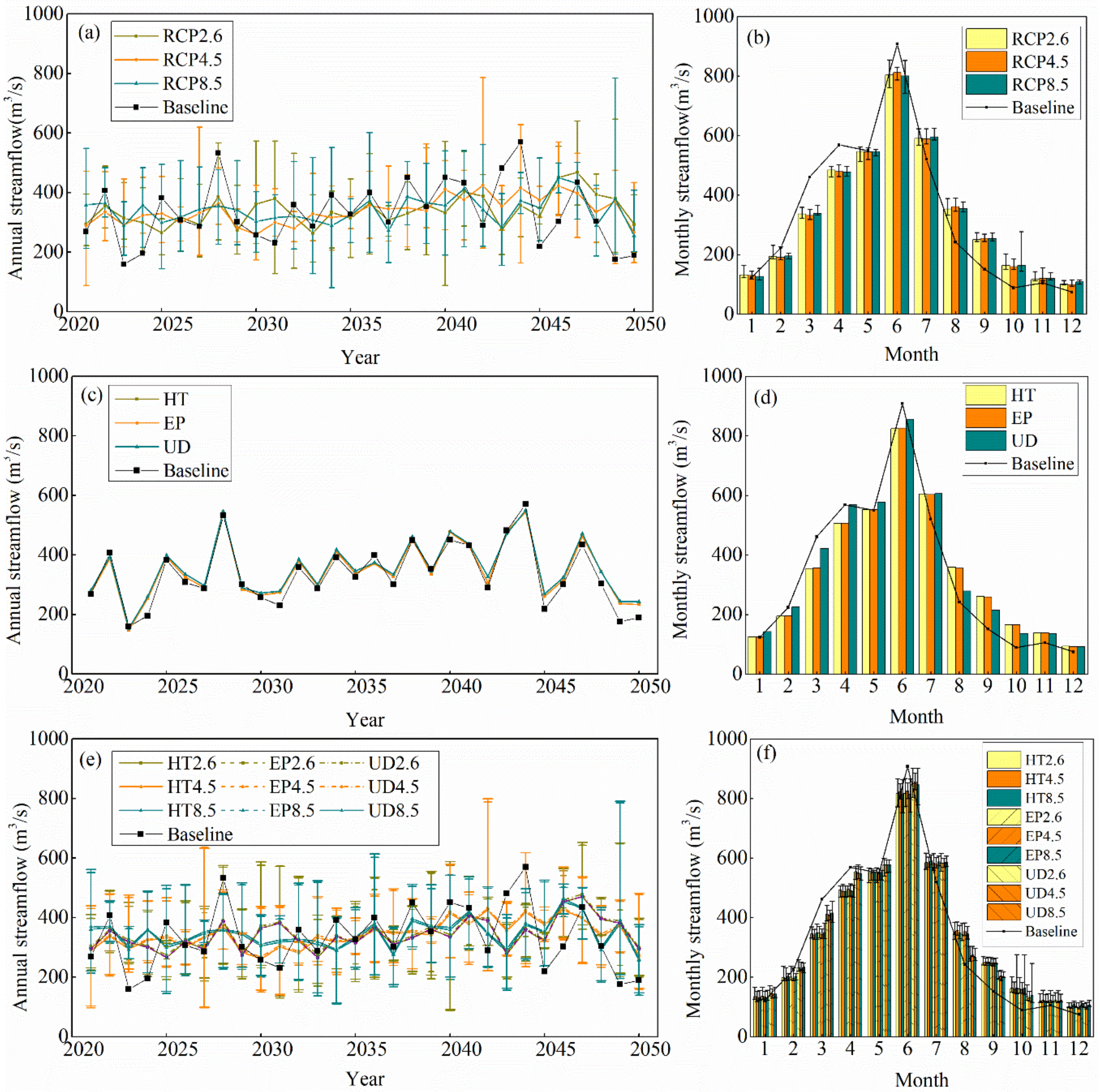

Fig. 4. Mean annual and monthly streamflow in Xinanjiang Basin in 2021-2050 under (a)-(b) climate change, (c)-(d) land use/cover change, and (e)-(f) combined climate and land use/cover change. The error bars indicate the multi-model ensemble range.

4. Discussion

4.1 Uncertainty analysis of streamflow

We used the fuzzy extension principle method to describe the streamflow uncertainty. The uncertainties at various levels resulted from the uncertainties or ranges in the GCM projections and land use/cover information in our study. Here the uncertainty in streamflow was computed at the α-cut values of 0%, 25%, 50%, and 75%, therefore the corresponding uncertainty levels were 100%, 75%, 50%, and 25%, respectively.

As shown in Fig. 5, the maximum variation in monthly streamflow occurs in October, and ranges from 125.17 to 258.40 m^3/s, while the minimum variation is observed in November and December, with a value of 26.72-32.86 m^3/s. The results show that annual streamflow in the baseline (1976-2005) is 334.86 m^3/s, and in the future (2021-2050), the mean annual streamflow under all scenarios is projected to be 345.69 m^3/s. The baseline streamflow exceeds the upper bounds in the flood seasons in March and June and the lower bounds in the non-flood seasons from September to December. The streamflow is concentrated mainly from April to July in both the baseline and the future periods. However, the future streamflow migrates from April to May and from June to July, resulting in a lower and more uniformly distributed streamflow in the flood seasons. This result corresponds to the phenomenon that GCM projections may underestimate the probability of extreme flooding (Malhi et al., 2009; Pervez and Henebry, 2014; Supharatid, 2015). In addition, the increased streamflow in the main non-flood seasons from October to December, with a significant value of 24.35-96.09%, contributes to a more blurred boundary between the flood and non-flood seasons. This result means that operating Xinanjiang Reservoir for water supply or hydropower generation might be easier in the future.

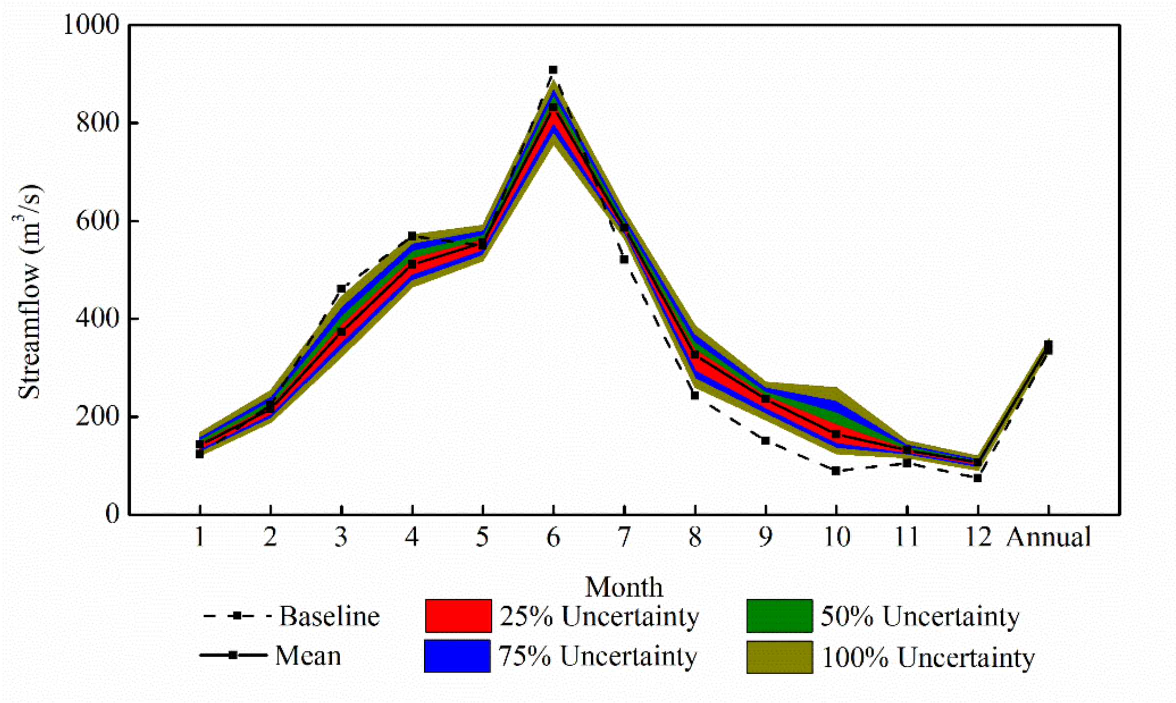

Fig. 5. Uncertainties of streamflow.

4.2 Attributing streamflow change to climate and land use/cover change

In this study, we first analyzed the individual and joint contributions of climate and land use/cover change to mean monthly streamflow change in Xinanjiang Basin. We used the multi-model ensemble means to eliminate the inter-model uncertainties under different RCPs. The RCA of streamflow attributed to climate change, land use/cover change, and combination is defined as the ratio of the change in streamflow under RCPs, land use/cover change (i.e., HT, EP, and UD) and combined conditions (i.e., HTs, EPs, UDs) in 2021-2050 relative to that in 1976-2005 to the standard deviation of streamflow in 1976-2005, respectively. The results are shown in Fig. 6.

Overall, climate change is one of the primary factors that influences the variation in streamflow. Although streamflow shows an increasing trend with increasing radiation intensity relative to the baseline streamflow, the RCA under RCPs is not sensitive to radiation intensity.

The maximum mean RCA occurs under RCP2.6, followed by that under RCP8.5 and RCP4.5. The impacts of climate change on streamflow are mainly realized through increased precipitation and temperature with a mean RCA of 0.34, 0.33, and 0.33 under the effects of RCP2.6, RCP4.5 and RCP8.5, respectively. In addition, the streamflow is concentrated mainly from May to July, it is less affected by climate change and thus has a lower bound of < 0.18 compared with that in the other months, especially in the non-flood seasons from September to October. Wen et al. (2018) and Wang et al. (2019b) also had the similar conclusion when evaluating the future streamflow variation induced by RCPs in southeastern China.

Furthermore, we find that streamflow induced by HT or EP has similar changes to that affected by climate change, with a mean RCA of 0.32 and 0.33, respectively; however, the streamflow under UD has a lower mean value of 0.20. As we mentioned before, the land use/cover in Xinanjiang Basin has undergone dramatic changes because of the sharp increase in urbanization. In this case, the UD with strong urbanization is more consistent with the baseline than the HT in terms of monthly streamflow. Zhang and Wei (2012) indicated that the decreasing forest reduces evaporation and interception, and causes increases in soil water content and groundwater re-charge, finally resulting in an increase in low flow. However, the streamflow under EP slightly increases due to the combined effects of the decreased forestland and increased grassland in our study.

The streamflow is less affected in non-flood seasons from September to October under UDs, which is similar to that under the effect of only UD; however, the streamflow is significantly altered in this period under the effects of HTs or EPs, which is similar to that under climate change alone. Accordingly, the combined impacts of climate and land use/cover changes on mean monthly streamflow are sensitive to IA. The impacts of climate change are stronger than those induced by land use/cover change under EP (i.e., lower IA), and land use/cover change has a greater impact in the case of UD (i.e., higher IA). The lack of observed significant changes in streamflow between HTs and EPs demonstrates that an increase in vegetation coverage does not contribute to the streamflow variation as much as IA does in Xinanjiang Basin.

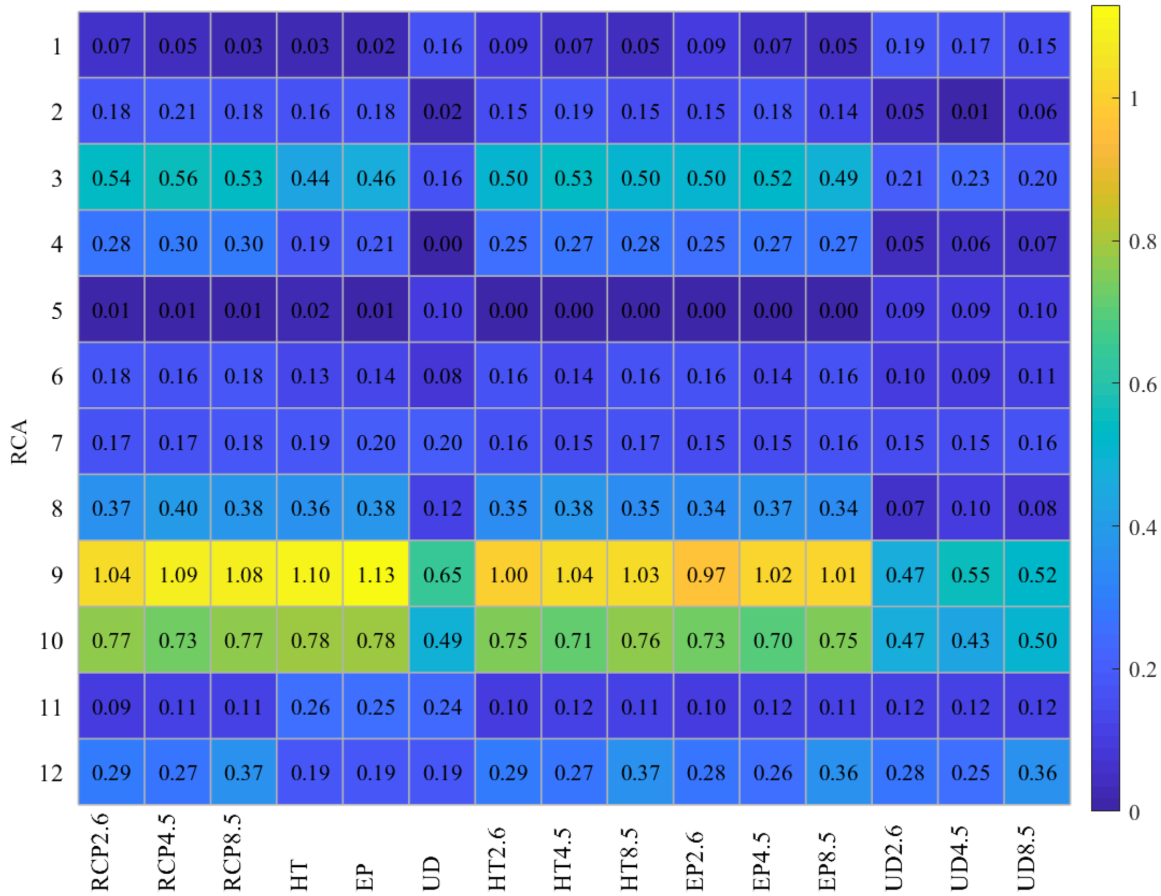

Fig. 6. Monthly RCA of streamflow attributed to climate change, land use/cover change, and combined climate and land use/cover change effects in Xinanjiang Basin.

We then quantified the contribution of climate and land use/cover changes impacting streamflow at the mean annual scale. The results listed in Table 3 show that the joint climate and land use/cover changes cause an increase in the mean annual streamflow of 6.35-13.61 m^3/s. The mean annual streamflow is expected to increase under both climate change alone and land use/cover change alone, but under the combined conditions it is lower than that of individual land use/cover influence, and higher than that of individual climate change influence. These results are because the complex and non-additive interactions between streamflow and climate change and land use/cover change in the future. Changes in mean annual streamflow will be mainly driven by land use/cover change, and climate change might weaken the influence on streamflow attributed to land use/cover change. Specifically, the land use/cover change leads to an increase in annual streamflow by 7.32-13.83 m^3/s, with a contribution of 101.60-115.37%, while the climate change decreases the annual streamflow by 0.22-0.99 m^3/s, with a contribution ranging from -15.37% to -1.60%. RCP8.5 has smaller effects in decreasing the influence on streamflow attributed to land use/cover change than does RCP2.6 and RCP4.5. However, under different catchments, different break points, different methods or even different time periods, the results may be different. The dominant effects of land use/cover change found in our study is consistent with the study by Berihun et al. (2019) and Yang et al. (2012), who both found that land use/cover change had a more pronounced effect than climate change on mean annual streamflow in Ethiopia and China, respectively. The opposite was found by Shrestha et al. (2018) in Thailand, and by El-Khoury et al. (2015) in Canada, who reported that climate variability had a greater effect than land use/cover change on annual streamflow response.

Table 3 Annual contributions of climate change and land use/cover change in Xinanjiang Basin.

Scenarios	HT2.6	EP2.6	UD2.6	HT4.5	EP4.5	UD4.5	HT8.5	EP8.5	UD8.5
Climate change (%)	-13.55	-14.67	-7.86	-14.09	-15.37	-8.14	-3.30	-3.64	-1.60
Land use change (%)	113.55	114.67	107.86	114.09	115.37	108.14	103.30	103.64	101.60
Total (%)	100.00	100.00	100.00	100.00	100.00	100.00	100.00	100.00	100.00

5 Conclusions

This study implemented a systematic framework consisting of scenarios design, climate and land use/cover change projection, streamflow response modelling and assessment, to quantify and characterize future streamflow variations in Xinanjiang Basin attributed to the individual and combined effects of climate and land use/cover changes. The main conclusions are summarized as follows:

(1) Climate in 2021-2050 was projected to be wetter and almost warmer relative to that in 1976-2005 in the target region. The areas of forest and grassland under EP were projected to undergo the largest proliferation among all scenarios from 1995 to 2025, while the area of urban land was the lowest; the land use/cover change under UD was on the contrary of that under EP. The land use/cover under HT would undergo dramatic changes following the historical trend, but experience less urbanization than that under UD.

(2) While both land use/cover change alone and combined changes projected an increase in streamflow (relative change: 3.89-5.81%, and 0.32-8.72%), there was a disagreement on the direction of streamflow change under climate change alone (relative change: -0.16-6.42%). The increased streamflow in the main non-flood seasons from October to December contributed to a more blurred boundary between the flood and non-flood seasons, which might potentially ease the operation stress of Xinanjiang Reservoir for water supply or hydropower generation.

(3) The impacts of climate change and land use/cover change on mean monthly streamflow was sensitive to IA: climate change was the dominant factor when the IA was smaller under HT and EP, whereas the land use/cover change was more dominant when the IA was larger under UD. However, changes in the mean annual streamflow were mainly driven by land use/cover change, and climate change might decrease the influence on streamflow attributed to land use/cover change. The contribution of climate change to decrease annual streamflow was -15.37-1.60%, while the contribution of land use/cover change to increase was 101.60-115.37%.

This study contributes to a better understanding the possible effects of climate and land use/cover changes on streamflow in Xinanjiang Basin and can therefore benefit greatly decision makers to design and implement possible adaptation actions for reservoir operations under environmental changes including both climate and land use/cover changes. Moreover, the approach of this study is beneficial for evaluating the combined effects of climate and land use/cover changes on basin hydrology and can be applied to other regions encountering similar pressures from environmental changes.

Acknowledgements

This research is funded by National Key Research and Development Plan "Inter-governmental Cooperation in International Scientific and Technological Innovation" (2016YFE0122100). We would like to acknowledge the insightful comments from the editors and anonymous reviewers.

References

Abbaspour, K. C., Vejdani, M., Haghighat, S. 2007. SWAT-CUP calibration and uncertainty programs for SWAT. Modsim International Congress on Modelling & Simulation Land Water & Environmental Management Integrated Systems for Sustainability, 364(3), 1603-1609.

Abera, W., Tamene, L., Abegaz, A., Solomon, D. 2019. Understanding climate and land surface changes impact on water resources using Budyko framework and remote sensing data in Ethiopia. Journal of Arid Environments, 167, 56-64.

Ahn, K.-H., Merwade, V. 2014. Quantifying the relative impact of climate and human activities on streamflow. Journal of Hydrology, 515, 257-266.

Alaoui, A., Willimann, E., Jasper, K., Magnusson, J., Weingartner, R. 2014. Modelling the Effects of Land Use and Climate Changes on Hydrology in the Ursern Valley, Switzerland. Hydrological Processes, 28(10), 3602-3614.

Anand, J., Gosain, A. K., Khosa, R. 2018. Prediction of land use changes based on Land Change Modeler and attribution of changes in the water balance of Ganga basin to land use change using the SWAT model. Science of the Total Environment, 644, 503-519.

Arnold, J. G., Srinivasan, R., Muttiah, R. S., Williams, J. R. 1998. Large Area Hydrologic Modeling and Assessment Part I: Model Development 1. Journal of the American Water Resources Association, 34(1), 73-89.

Behera, M. D., Borate, S. N., Panda, S. N., Behera, P. R., Roy, P. S. 2012. Modelling and analyzing the watershed dynamics using Cellular Automata (CA)--Markov model - A geo-information based approach. Journal of Earth System Science, 121(4), 1011-1024.

Berihun, M. L., Tsunekawa, A., Haregeweyn, N., Meshesha, D. T., Adgo, E., Tsubo, M., et al. 2019. Hydrological responses to land use/land cover change and climate variability in contrasting agro-ecological environments of the Upper Blue Nile basin, Ethiopia. Science of the Total Environment, 689, 347-365.

Bhatta, B., Shrestha, S., Shrestha, P. K., Talchabhadel, R. 2019. Evaluation and application of a SWAT model to assess the climate change impact on the hydrology of the Himalayan River Basin. CATENA, 181, 104082.

Chase, K. J., Haj, A. E., Regan, R. S., Viger, R. J. 2016. Potential effects of climate change on streamflow for seven watersheds in eastern and central Montana. Journal of Hydrology: Regional Studies, 7, 69-81.

Chen, L., Frauenfeld, O. W. 2014. A comprehensive evaluation of precipitation simulations over China based on CMIP5 multimodel ensemble projections. Journal of Geophysical Research, 119(10), 5767-5786.

Clerici, N., Cote-Navarro, F., Escobedo, F. J., Rubiano, K., Villegas, J. C. 2019. Spatio-temporal and cumulative effects of land use-land cover and climate change on two ecosystem services in the Colombian Andes. Science of the Total Environment, 685, 1181-1192.

Cubasch, U., Wuebbles, D., Chen, D., Facchini, M. C., Frame, D., Mahowald, N., et al. 2013. Introduction. In: Climate Change 2013: The Physical Science Basis. Contribution of Working Group I to the Fifth Assessment Report of the Intergovernmental Panel on Climate Change. Computational Geometry.

Deliman, P. N., Pack, W. J., Nelson, E. J. 1999. Integration of the Hydrologic Simulation Program-FORTRAN (HSPF) watershed water quality model into the Watershed Modeling System (WMS).

Dile, Y. T., Daggupati, P., George, C., Srinivasan, R., Arnold, J. 2016. Introducing a new open source GIS user interface for the SWAT model. Environmental Modelling & Software, 85, 129-138.

Eisner, S., Flörke, M., Chamorro, A., Daggupati, P., Donnelly, C., Huang, J., et al. 2017. An ensemble analysis of climate change impacts on streamflow seasonality across 11 large river basins. Climatic Change, 141(3), 401-417.

El-Khoury, A., Seidou, O., Lapen, D. R., Que, Z., Mohammadian, M., Sunohara, M., et al. 2015. Combined impacts of future climate and land use changes on discharge, nitrogen and phosphorus loads for a Canadian river basin. Journal of environmental management, 151, 76-86.

Firozjaei, M. K., Sedighi, A., Argany, M., Jelokhani-Niaraki, M., Arsanjani, J. J. 2019. A geographical direction-based approach for capturing the local variation of urban expansion in the application of CA-Markov model. Cities, 93, 120-135.

Flanagan, D. C., Ascough, J. C., Nearing, M. A., Laflen, J. M. 2001. The Water Erosion Prediction Project (WEPP) Model. Boston, MA: Springer US.

Gao, P., Jiang, G., Wei, Y., Mu, X., Wang, F., Zhao, G., et al. 2015. Streamflow regimes of the Yanhe River under climate and land use change, Loess Plateau, China. Hydrological Processes, 29(10), 2402-2413.

Gonzalez, A., Pons, O., Vila, M. A. 1999. Dealing with uncertainty and imprecision by means of fuzzy numbers. International Journal of Approximate Reasoning, 21(3), 233-256.

Guo, Y., Fang, G., Wen, X., Lei, X., Yuan, Y., Fu, X. 2019. Hydrological responses and adaptive potential of cascaded reservoirs under climate change in Yuan River Basin. Hydrology Research, 50(1), 358-378.

Kendall, M. G. 1975. Rank Correlation Methods. Charles Griffin, London.

Kim, J., Choi, J., Choi, C., Park, S. 2013. Impacts of changes in climate and land use/land cover under IPCC RCP scenarios on streamflow in the Hoeya River Basin, Korea. Science of the Total Environment, 452-453, 181-195.

Li, C., Liu, M., Hu, Y., Shi, T., Qu, X., Walter, M. T. 2018. Effects of urbanization on direct runoff characteristics in urban functional zones. Science of the Total Environment, 643, 301-311.

Liang, X., Lettenmaier, D. P., Wood, E. F., Burges, S. J. 1994. A simple hydrologically based model of land surface water and energy fluxes for general circulation models. Journal of Geophysical Research: Atmospheres, 99(D7), 14415-14428.

Liu, X., Ren, L., Yuan, F., Singh, V. P., Fang, X., Yu, Z., et al. 2009. Quantifying the effect of land use and land cover changes on green water and blue water in northern part of China. Hydrology and Earth System Sciences, 13(6), 735-747.

Malhi, Y., Aragão, L. E. O. C., Galbraith, D., Huntingford, C., Fisher, R., Zelazowski, P., et al. 2009. Exploring the likelihood and mechanism of a climate-change-induced dieback of the Amazon rainforest. Proceedings of the National Academy of Sciences, 106(49), 20610.

Mann, H. B. 1945. Non-Parametric Test Against Trend. Econometrica, 13(3), 245-259.

Mito, Y., Ismail, M. A. M., Yamamoto, T. 2011. Multidimensional scaling and inverse distance weighting transform for image processing of hydrogeological structure in rock mass. Journal of Hydrology, 411(1), 25-36.

Mitsova, D., Shuster, W., Wang, X. 2011. A cellular automata model of land cover change to integrate urban growth with open space conservation. Landscape and Urban Planning, 99(2), 141-153.

Molina-Navarro, E., Trolle, D., Martínez-Pérez, S., Sastre-Merlín, A., Jeppesen, E. 2014. Hydrological and water quality impact assessment of a Mediterranean limno-reservoir under climate change and land use management scenarios. Journal of Hydrology, 509, 354-366.

Neupane, R. P., White, J. D., Alexander, S. E. 2015. Projected hydrologic changes in monsoon-dominated Himalaya Mountain basins with changing climate and deforestation. Journal of Hydrology, 525, 216-230.

Ning, T., Li, Z., Liu, W. 2016. Separating the impacts of climate change and land surface alteration on runoff reduction in the Jing River catchment of China. CATENA, 147, 80-86.

Pan, Y., Luo, Y., Wang, Y., Zhang, Q., Zhu, Z. 2018. Characteristics of Evolution of Precipitation and Runoff in Xin'An River Basin. Research of Soil and Water Conservation, 25(6), 121-125.

Pervez, M. S., Henebry, G. M. 2014. Projections of the Ganges–Brahmaputra precipitation—Downscaled from GCM predictors. Journal of Hydrology, 517, 120-134.

Pettitt, A. N. 1979. A Non-Parametric Approach to the Change-Point Problem. Journal of the Royal Statistical Society. Series C (Applied Statistics), 28(2), 126-135.

Qiang, Z., Xiao, M., Singh, V. P., Lin, L., Chong-Yu. 2016. Evaluation of impacts of climate change and human activities on streamflow in the Poyang Lake basin, China. Hydrological Processes, 30(14), 2562-2576.

Ruelland, D., Ardoin-Bardin, S., Collet, L., Roucou, P. 2012. Simulating future trends in hydrological regime of a large Sudano-Sahelian catchment under climate change. Journal of Hydrology, 424-425, 207-216.

Sang, L., Zhang, C., Yang, J., Zhu, D., Yun, W. 2011. Simulation of land use spatial pattern of towns and villages based on CA–Markov model. Mathematical and Computer Modelling, 54(3), 938-943.

Shepard, D. S. 1984. Computer Mapping: The SYMAP Interpolation Algorithm. In G. L. Gaile & C. J. Willmott (Eds.), Spatial Statistics and Models. Springer Netherlands, Dordrecht, 133-145.

Shi, X. 2013. Study on distributed hydrological simulation and drought evaluation method in Luanhe river basin based on SWAT model[D]. University of Chinese Academy of Sciences, Beijing, China.

Shrestha, S., Bhatta, B., Shrestha, M., Shrestha, P. K. 2018. Integrated assessment of the climate and landuse change impact on hydrology and water quality in the Songkhram River Basin, Thailand. Science of the Total Environment, 643, 1610-1622.

Sun, Q., Miao, C., Duan, Q. 2016. Extreme climate events and agricultural climate indices in China: CMIP5 model evaluation and projections. International Journal of Climatology, 36(1), 43-61.

Supharatid, S. 2015. Assessment of CMIP3-CMIP5 Climate Models Precipitation Projection and Implication of Flood Vulnerability of Bangkok. American Journal of Climate Change, 140-162.

Suriya, S., Mudgal, B. V. 2012. Impact of urbanization on flooding: The Thirusoolam sub watershed - A case study. Journal of Hydrology, 412-413, 210-219.

Thrasher, B., Maurer, E. P., McKellar, C., Duffy, P. B. 2012. Technical Note: Bias correcting climate model simulated daily temperature extremes with quantile mapping. Hydrology and Earth System Sciences, 16(9), 3309-3314.

Trolle, D., Nielsen, A., Andersen, H. E., Thodsen, H., Olesen, J. E., Børgesen, C. D., et al. 2019. Effects of changes in land use and climate on aquatic ecosystems: Coupling of models and decomposition of uncertainties. Science of the Total Environment, 657, 627-633.

Umair, M., Kim, D., Choi, M. 2019. Impacts of land use/land cover on runoff and energy budgets in an East Asia ecosystem from remotely sensed data in a community land model. Science of the Total Environment, 684, 641-656.

Wambura, F. J., Ndomba, P. M., Kongo, V., Tumbo, S. D. 2015. Uncertainty of runoff projections under changing climate in Wami River sub-basin. Journal of Hydrology Regional Studies, 4, 333-348.

Wang, H., Tetzlaff, D., Soulsby, C. 2018. Modelling the effects of land cover and climate change on soil water partitioning in a boreal headwater catchment. Journal of Hydrology, 558, 520-531.

Wang, X., He, K., Dong, Z. 2019a. Effects of climate change and human activities on runoff in the Beichuan River Basin in the northeastern Tibetan Plateau, China. CATENA, 176, 81-93.

Wang, Y., Lei, X., Wen, X., Fang, G., Tan, Q., Tian, Y., et al. 2019b. Effects of damming and climatic change on the eco-hydrological system: A case study in the Yalong River, southwest China. Ecological Indicators, 105, 663-674.

Wei, L. J., Xiaohui, Q., Junfang, L., Fei, A. 2010. The high frequency characteristic of amorphous iron induction motor. International Conference on Computer and Communication Technologies in Agriculture Engineering, Chengdu.

Wen, X., Liu, Z., Lei, X., Lin, R., Fang, G., Tan, Q., et al. 2018. Future changes in Yuan River ecohydrology: Individual and cumulative impacts of climates change and cascade hydropower development on runoff and aquatic habitat quality. Science of the Total Environment, 633, 1403-1417.

Woldesenbet, T. A., Elagib, N. A., Ribbe, L., Heinrich, J. 2017. Hydrological responses to land use/cover changes in the source region of the Upper Blue Nile Basin, Ethiopia. Science of the Total Environment, 575, 724-741.

Woldesenbet, T. A., Elagib, N. A., Ribbe, L., Heinrich, J. 2018. Catchment response to climate and land use changes in the Upper Blue Nile sub-basins, Ethiopia. Science of the Total Environment, 644, 193-206.

Yang, W., Long, D., Bai, P. 2019. Impacts of future land cover and climate changes on runoff in the mostly afforested river basin in North China. Journal of Hydrology, 570, 201-219.

Yang, X., Ren, L., Singh, V. P., Liu, X., Yuan, F., Jiang, S., et al. 2012. Impacts of land use and land cover changes on evapotranspiration and runoff at Shalamulun River watershed, China. Hydrology Research, 43(1-2), 23-37.

Yin, J., He, F., Xiong, Y. J., Qiu, G. Y. 2017a. Effect of land use/land cover and climate changes on surface runoff in a semi-humid and semi-arid transition zone in Northwest China. Hydrology and Earth System Sciences, 21, 1-23.

Yin, J., He, F., Xiong, Y. J., Qiu, G. Y. 2017b. Effects of land use/land cover and climate changes on surface runoff in a semi-humid and semi-arid transition zone in northwest China. Hydrology and Earth System Sciences, 21(1), 183-196.

Zhang, L., Bai, K. Z., Wang, M. J., Karthikeyan, R. 2016. Basin-scale spatial soil erosion variability: Pingshuo opencast mine site in Shanxi Province, Loess Plateau of China. Natural Hazards, 80(2), 1213-1230.

Zhang, L., Karthikeyan, R., Bai, Z., Srinivasan, R. 2017. Analysis of streamflow responses to climate variability and land use change in the Loess Plateau region of China. CATENA, 154, 1-11.

Zhang, M., Wei, X. 2012. The effects of cumulative forest disturbance on streamflow in a large watershed in the central interior of British Columbia, Canada. Hydrology and Earth System Sciences, 16(7), 2021-2034.

Zhang, Y., Xia, J., Yu, J., Randall, M., Zhang, Y., Zhao, T., et al. 2018. Simulation and assessment of urbanization impacts on runoff metrics: insights from landuse changes. Journal of Hydrology, 560, 247-258.

Zhao, M., He, Z., Du, J., Chen, L., Lin, P., Fang, S. 2019. Assessing the effects of ecological engineering on carbon storage by linking the CA-Markov and InVEST models. Ecological Indicators, 98, 29-38.

Zheng, H., Chiew, F. H. S., Charles, S., Podger, G. 2018. Future climate and runoff projections across South Asia from CMIP5 global climate models and hydrological modelling. Journal of Hydrology: Regional Studies, 18, 92-109.

Zheng, Y., Wn, X., FANG, G. 2015. Research on climate change and runoff response in Xin'an river basin. Journal of Water Resources and Water Engineering, 26(1), 106-110.

Zuo, D., Xu, Z., Yao, W., Jin, S., Xiao, P., Ran, D. 2016. Assessing the effects of changes in land use and climate on runoff and sediment yields from a watershed in the Loess Plateau of China. Science of the Total Environment, 544, 238-250.